First-principles investigation on interface bonding properties between $Fe_3Cr_3YC_3$ and γ-Fe

Yuenian He [a], Jun Liu [b], Wei Shao [a], Lixiang Rao [a], Silong Zhang [a], Xuejun Ren [c], Qingxiang Yang [a]

[a] State Key Lab of Metastable Materials Science & Technology, Hebei Key Lab for Optimizing Metal Product Technology and Performance, Yanshan University, Qinhuangdao 066004, PR China

[b] Department of Environmental Engineering, Hebei University of Environmental Engineering, Qinhuangdao 066102, PR China

[c] School of Engineering, Liverpool John Moores University, Liverpool L3 3AF, UK

Abstract

We performed a first-principles calculation to investigate the interface bonding properties between $Fe_3Cr_3YC_3$ and γ-Fe crystal structures. The study shows that the lattice mismatch of $Fe_3Cr_3YC_3(10\,\bar{1}\,0)$/γ-Fe(1 1 1) interface is 5.02 %. Four interface structures named as Fe-Fe, Cr-Fe, C-Fe and Y-Fe were established. Among them, the bonding work of Y-Fe interface is the largest(0.370 J/m^2), and its interface energy is the smallest(-0.3397 J/m^2). The charge-aggregation region of Y-Fe interface is larger than those of Fe-Fe, Cr-Fe and C-Fe. It reveals that the Y-Fe interface in $Fe_3Cr_3YC_3(10\,\bar{1}\,0)$/γ-Fe(1 1 1) interfaces is the most stable.

Keywords

Interface, Crystal structure, $Fe_3Cr_3YC_3$, γ-Fe, First principles calculation

1. Introduction

Because of high hardness and excellent wear resistance, hypereutectic Fe-Cr-C alloy have been applied in the additive manufacturing fields [1]. By hardfacing method, this alloy can be cladded on the surface to prepare the various shape wear-resistant workpieces [2]. The excellent wear resistance of this alloy is mainly depend on the presence of primary M_7C_3 (M = Fe, Cr) carbide, when Fe:Cr = 3:4(namely $Fe_3Cr_4C_3$), the crystal structure is the most stable [3], [4]. However, when its sizes are large, the interface bonding properties between $Fe_3Cr_4C_3$ carbide and austenite (γ-Fe) are poor, and cracks can easily appear in the interface. Therefore, the service life of the workpieces is seriously shortened [5].

With modifying, purifying and alloying effectiveness [6], [7], rare earth oxide, such as Y_2O_3 has been applied in the hypereutectic Fe-Cr-C alloy to refine its microstructure and improve its wear resistance [8]. The Y doping in this alloy can improve the plasticity and

toughness [9]. However, it is not clear that the effect of Y doping on the interface bond strength and anti-cracking performance. Moreover, it is difficult to determine the interfacial relationship between $Fe_3Cr_4C_3$ and γ-Fe by experimental.

In recent years, the first-principles has been used to investigate the interfacial relationships [10], [11]. In this paper, Y was used as a doping element to form $Fe_3Cr_3YC_3$. The bonding work and interfacial energy of $Fe_3Cr_3YC_3$/γ-Fe interfaces were calculated, and interfacial charge density difference was analyzed by first-principles. The bonding mechanism of $Fe_3Cr_3YC_3$/γ-Fe interface was elaborated at atomic scale.

2. Methodology

The bulk properties of $Fe_3Cr_3YC_3$ and γ-Fe structures were calculated using Vienna Ab-initio Simulation Package to optimize their structures and calculate their surface and interface properties. The generalized gradient approximation functional was improved by Perdew, Burke and Ernzerhorf, which was used to calculate and modify the exchange correlation energy [12]. In the convergence test, the energy convergence criterion was set to 1×10^{-5} eV/atom and the force convergence criterion to 0.02 eV/Å, resulting in suitable plane wave cutoff energy (E_{cut}) and K-point mesh (K_{mesh}) in the Brillouin zone.

3. Results and discussion

$Fe_3Cr_4C_3$ is a hexagonal system and belongs to *P*63*mc* space group. The optimized lattice constants are a = b = 7.004 Å and c = 4.275 Å. According to the calculations for Y-atom doped $Fe_3Cr_4C_3$ carbide [13], the total structural energy is the lowest when the Y at the Wyckoff 2b position, the crystal structure is the most stable. The optimization calculation results of $Fe_3Cr_3YC_3$ crystal models show that the lattice constants are a = b = 7.033 Å, c = 4.295 Å. γ-Fe is a cubic system and belongs to the *Fm*3*m* space group. The optimized lattice constants of γ-Fe are a = b = c = 3.449 Å. The crystal structures of $Fe_3Cr_3YC_3$ and γ-Fe are shown in Fig. 1.

The Bramfitt lattice mismatch theory [14] was used to calculate the lattice mismatches between $Fe_3Cr_3YC_3$ and γ-Fe crystal structures. Since $Fe_3Cr_3YC_3$ is obtained by replacing the atoms in $Fe_3Cr_4C_3$ with the Y atoms, the selection of $Fe_3Cr_4C_3$ can be used in selecting the

surface. According to the experimental results in [15], the γ-Fe(1 1 1) and $Fe_3Cr_4C_3$(10 1^{-} 0) planes were selected for the study. Meanwhile, the calculated lattice mismatch between $Fe_3Cr_3YC_3$ (10 1^{-} 0) and γ-Fe (1 1 1) planes is 5.02 %. It reveals that $Fe_3Cr_3YC_3$ (10 1^{-} 0)/γ-Fe (1 1 1) interface is very effective heterogeneous nucleation one. Therefore, $Fe_3Cr_3YC_3$(10 1^{-} 0) and γ-Fe(1 1 1) are selected to construct interface models.

Based on above calculations, the $Fe_3Cr_3YC_3$(10 1^{-} 0) and γ-Fe(1 1 1) were selected to establish the surface model. The surface models of $Fe_3Cr_3YC_3$(10 1^{-} 0) and γ-Fe(1 11) are shown in Fig. 2. Fig. 2(a)–(d) are the four different surface termination models of Fe, Cr, C, and Y in $Fe_3Cr_3YC_3$(10 1^{-} 0) plane, respectively, and Fig. 2(e) is γ-Fe(1 11) plane.

To ensure that the surface models reflect the internal characteristics of the bulk phase, the surface models need to be tested for convergence. In order to eliminate the dipole effect, the atom types on the upper are consistent with the lower surfaces of the configuration, and different types of atoms will not conform to the stoichiometric ratio. Therefore, the convergence of the interatomic spacing of the cell configuration with increase of atomic layer number was used to determine the minimum number of atomic layers required to maintain the bulk phase. The calculated results show that Fe, Cr surface termination models are converged at the 43th layer, and C, Y are at the 29 h. Using the same method, γ-Fe (1 1 1) surface is at the 7th.

Four interface termination models were constructed, named as Fe-Fe, Cr-Fe, C-Fe and Y-Fe, as shown in Fig. 3. Fig. 3(a)–(d) and (a')-(d') are the interface structure and its vertical view. Fig. 3(a)-(a') shows that the Fe at the corner is directly opposite the Fe. From Fig. 3(b)-(b'), the Cr at the corner is directly opposite the Fe. Fig. 3(c)-(c') shows that the C at the corner is directly opposite the Fe. From Fig. 3(d)-(d'), the Y at the corner is directly opposite the Fe.

For four termination models of Fe-Fe, Cr-Fe, C-Fe, and Y-Fe, the total energy has a maximum when their interface spacing are 1.8 Å, 1.6 Å, 2.0 Å, 1.8 Å, respectively, which indicates that the interface structure is the most stable.

Adhesion work (W_{ad}) is defined as the reversible work of energy required to separate an interface into two free surfaces, which is used as a measure of the interface bonding strength [16]. The higher the W_{ad} is, the stronger the interface is and the more stable the structure is. The equation is as follows [17]:

$$W_{ad} = \frac{E_{Fe} + E_{Fe_3Cr_3YC_3} - E_{\gamma-Fe/Fe_3Cr_3YC_3}}{A} \quad (1)$$

where $E_{\gamma-Fe}$ and $E_{Fe3Cr3YC3}$ are the total energy of the γ-Fe(111) and $Fe_3Cr_3YC_3$(10 1 0) surface, respectively; $E\gamma-Fe/Fe_3Cr_3YC_3$ is the total energy of the interface model; A is the interface area.

The calculated W_{ad}(J/m2) of Fe3Cr3YC3(10 1 0)/γ-Fe(111) interface are as follows:

$W_{ad}^{Y-Fe} = 0.3703$; $W_{ad}^{Cr-Fe} = 0.3483$; $W_{ad}^{Fe-Fe} = 0.3456$; $W_{ad}^{C-Fe} = 0.3440$, in which, WY− Fe ad is the largest.

Interfacial energy (γ) is another important criterion for determining whether a structure is stable or not. The smaller the γ is, the more stable the interfacial structure is. The equation is as follows [18]:

$$\gamma = \sigma_{Fe} + \sigma_{Fe_3Cr_3YC_3} - W_{ad} \quad (2)$$

where σFe and σFe3Cr3YC3 are the surface energy after relaxation of γ-Fe (111) surface configurations and Fe3Cr3YC3(10 1 0) one, respectively; Wad is the adhesion work of Fe3Cr3YC3(10 1 0)/γ-Fe (111) interface.

γ-Fe (111) surface is a nonpolar surface, the surface energy formula is as follows [19]:

$$\sigma_{Fe} = \frac{1}{2A}(E_{slab}^{N}\text{-N}\Delta\text{E}) \quad (3)$$

$$\Delta E = \frac{1}{2}(E_{slab}^{N} - E_{slab}^{N-2}) \quad (4)$$

where N is the number of atomic layers of the surface model; E is the total energy of the surface model of different layer.

$$\sigma_{Fe3Cr3YC3(10\bar{1}0)} = \frac{1}{2A}(E_{slab} - N_{Fe}\mu_{Fe}^{slab} - N_{Cr}\mu_{Cr}^{slab} - N_C\mu_C^{slab} - N_Y\mu_Y^{slab}) \quad (5)$$

where A is the surface area; E_{slab} is the total energy of the surface

configuration; N is the number of atoms in $Fe_3Cr_3YC_3$ surface configuration. μ is chemical potential in the bulk $Fe_3Cr_3YC_3$

Synthesizing Eqs. (1), (2), (3), (4) and (5), the calculated γ(J/m2) of Fe3Cr3YC3(10 1 0)/γ-Fe(111) interface are as follows: $\gamma_{Fe-Fe} = -0.3255$; $\gamma_{C-Fe} = -0.3283$; $\gamma_{Cr-Fe} = -0.3292$; $\gamma_{Y-Fe} = -0.3397$, in which, γ_{Y-Fe} is the smallest.

In order to further illustrate the bonding information between different atoms in the interface structures, the differential charge density (Δρ) was characterized for four interface termination models. The equation of Δρ is as follows [21]:

$$\Delta\rho = \rho_{total} - \rho_{Fe_3Cr_3YC_3(10\bar{1}0)} - \rho_{\gamma-Fe(111)} \quad (6)$$

where ρ_{total} represents the total charge density in the interface system; $\rho_{Fe3Cr3YC3(1010)}$ and $\rho_{\gamma-Fe(111)}$ represent the charge densities of isolate Fe3Cr3YC3(10 1 0) and γ-Fe(111) in the same interface, respectively.

The Δρ front view and side view of $Fe_3Cr_3YC_3$(10 1 0)/γ-Fe(111) interface are shown in Fig. 4, in which the dotted lines represent the interface position, and the positive value (red) represents charge ag gregation and negative value (blue) represents charge absence. From Fig. 4(a)-(a'), there is mainly a charge-rich region at Fe-Fe interface. A charge-deficient region around the Fe located below the interface, while the C located above the interface have a charge-aggregating region near the interface side. From Fig. 4(b)-(b'), the charge-aggregating region at Cr-Fe interface is located to the right of the interface. From Fig. 4(c)-(c'), the charge-aggregating regions exist on the left and right sides of the C Fe interface, and charge-deficient region appear in the middle. From Fig. 4(d)-(d'), there is mainly a charge-aggregating region at Y-Fe interface, while the small areas of charge deficiency on each of the left and right sides. Compared Fig. 4(d) with Fig. 4(a-c), the distances between Y and Fe at the interface are closer, and the charge-aggregation region is the largest, which indicates that the bond strength of Y-Fe interface is higher than those of other three interfaces.

4. Conclusions

In summary, the lattice mismatch between Fe3Cr3YC3(10 1 0) plane and γ-Fe(111) plane is 5.02 %. Fe3Cr3YC3(10 1 0) slabs and γ-Fe(111) slabs are selected to construct interface models. Four interfaces have been constructed named as Fe-Fe, Cr-Fe, C-Fe and Y-Fe. Among them, the bonding work of Y-Fe interface is the largest(0.370 J/m2), and its interface energy is the smallest(-0.3397 J/m2). The charge-aggregation region of Y-Fe interface is larger than those of Fe-Fe, Cr-Fe and C-Fe. It reveals that the Y-Fe interface in Fe3Cr3YC3(10 1 0)/γ-Fe(111) interfaces is the most stable, which indicates that Y-doping in Fe3Cr4C3 carbide can improve the interface bonding properties.

CRediT authorship contribution statement

Yuenian He: Conceptualization, Methodology, Investigation, Writing – original draft. Jun Liu: Supervision, Writing – review & editing. Wei Shao: Conceptualization, Methodology. Lixiang Rao: Methodology, Writing – review & editing. Silong Zhang: Writing – re view & editing. Xuejun Ren: Methodology, Writing – review & editing. Qingxiang Yang: Supervision, Funding acquisition, Writing – review & editing.

Declaration of Competing Interest

The authors declare that they have no known competing financial interests or personal relationships that could have appeared to influence the work reported in this paper.

Acknowledgments

The authors would like to express their gratitude for projects sup ported by the National Natural Science Foundation of China (No.51771167), Hebei Province Innovation Ability Promotion Project

(22567609H), European Union's Horizon 2020 Research and innovation program through a Marie Sklodowska-Curie Research and Innovation Staff Exchange Funding (Grant Agreement No.823786).

References

[1] X.J. Wu, J.D. Xing, H.G. Fu, X.H. Zhi, Mater. Sci. Eng. A 457 (2007) 180–185.
[2] V.E. Buchanan, P.H. Shipway, D.G. McCartney, Wear 263 (2007) 99–110.
[3] P. Zhang, Y. Zhou, J. Yang, D. Li, X. Ren, Y. Yang, Q. Yang, J. Alloys Compd. 560 (2013) 49–53.
[4] X.Y. Chong, M.Y. Hu, P. Wu, Q. Shan, Y.H. Jiang, Z.L. Li, J. Feng, Acta Mater. 169 (2019) 193–208.
[5] X. Zhi, J. Xing, H. Fu, B. Xiao, Mater. Lett. 62 (2008) 857–860.
[6] X.Z. Pang, J.B. Yang, M.J. Pang, Y.J. Zhao, W.C. Yang, J. Alloys Compd. 831 (2020) 154747.
[7] M.A. Lahmer, Appl. Surf. Sci. 457 (2018) 315–322.
[8] S. Liu, J. Zhang, Z.J. Wang, Z.J. Shi, Y.F. Zhou, X.J. Ren, Q.X. Yang, Mater. Charact. 132 (2017) 41–45.
[9] Z. Shi, W. Shao, L. Rao, T. Hu, X. Xing, Y. Zhou, S. Liu, Q. Yang, J. Alloys Compd. 850 (2021), 156656.
[10] G.Y. Yang, Y. Liu, Z.Q. Hang, N.Y. Xi, H. Fu, H. Chen, J. Rare Earths 37 (2019) 773–780.
[11] R.W. Li, Q.C. Chen, L.O. Yang, Y.J. Zhang, B.J. Nie, Y.L. Ding, Ceram. Int. 47 (2021) 22810–22820.
[12] J.P. Perdew, K. Burke, M. Ernzerhof, Phys. Rev. Lett. 77 (1996) 3865–3868.
[13] Z.J. Shi, W. Shao, L.X. Rao, T.S. Hu, X.L. Xing, Y. Zhou, S. Liu, Q. Yang, Appl. Surf. Sci. 538 (2021), 148108.
[14] B.L. Bramfitt, Metall. Trans. 1 (1970) 1987–1995.
[15] W. Shao, Y.F. Zhou, L. Zhou, L.X. Rao, X.L. Xing, Z.J. Shi, Q. Yang, Mater. Des. 211 (2021), 110133.
[16] L. Chen, Y.F. Li, Z.L. Zhao, Q.L. Zheng, D.W. Yi, X. Li, J. Jianhong Peng, J. Sun, Chem. Phys. 547 (2021), 111193. [
17] X. Pang, X. Yang, J. Yang, Y. Zhao, M. Pang, Diam. Relat. Mater. 113 (2021), 108297.
[18] R.W. Li, Q.C. Chen, L. Ouyang, Y.L. Ding, J. Alloys Compd. 870 (2021), 159529.
[19] J.C. Boettger, Phys. Rev. B 49 (1994) 16798–16800.
[20] Y. Wu, Y.H. Duan, X.L. Zhou, M.J. Peng, Surf. Interfaces 30 (2022), 101974.
[21] V. Fiorentini, M. Methfessel, J. Phys. Condens. Matter. 8 (1996) 6525–6529.

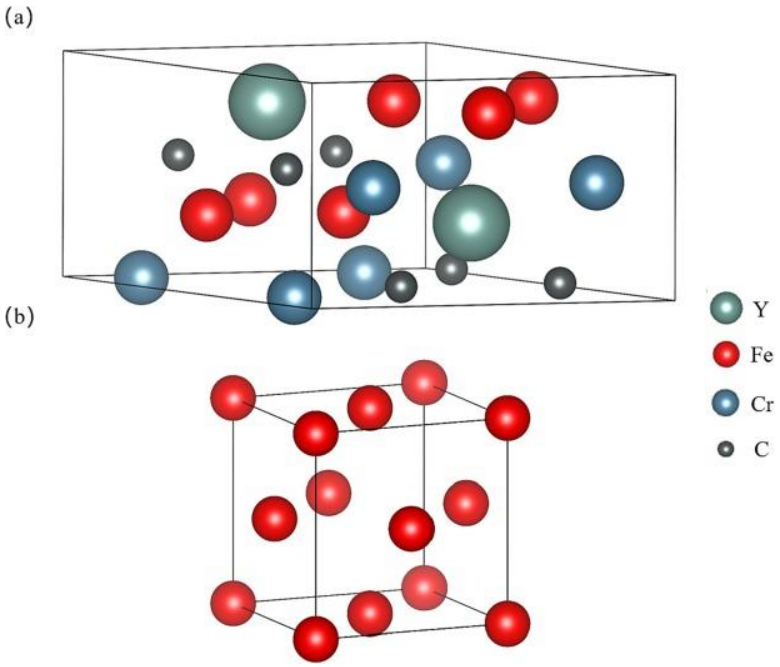

Fig. 1. Crystal structure: (a) $Fe_3Cr_3YC_3$; (b) γ-Fe.

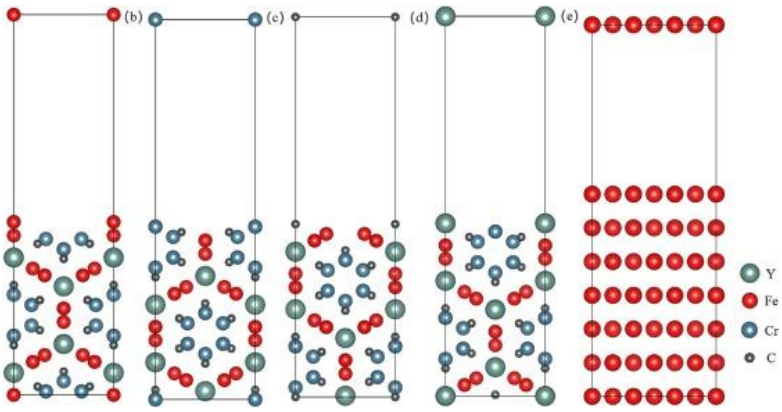

Fig. 2. Surface models of $Fe_3Cr_3YC_3(10\bar{1}0)$ and γ-Fe(111) plane: (a) Fe-termination surface model; (b) Cr-terminated surface model; (c) C-terminated surface model; (d) Y-terminated surface model; (e) γ-Fe(111) surface model.

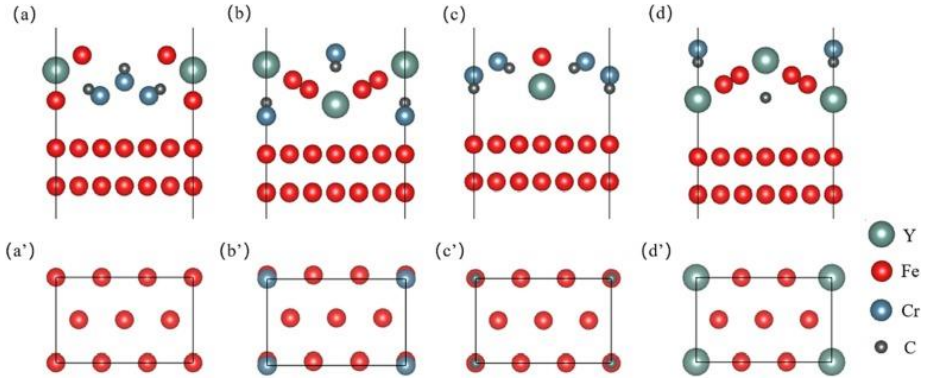

Fig. 3. Interface structures of $Fe_3Cr_3YC_3(10\bar{1}0)//\gamma$-Fe (1 1 1): (a),(a') Fe-Fe; (b),(b') Cr-Fe; (c),(c') C-Fe. (d), (d') Y-Fe.

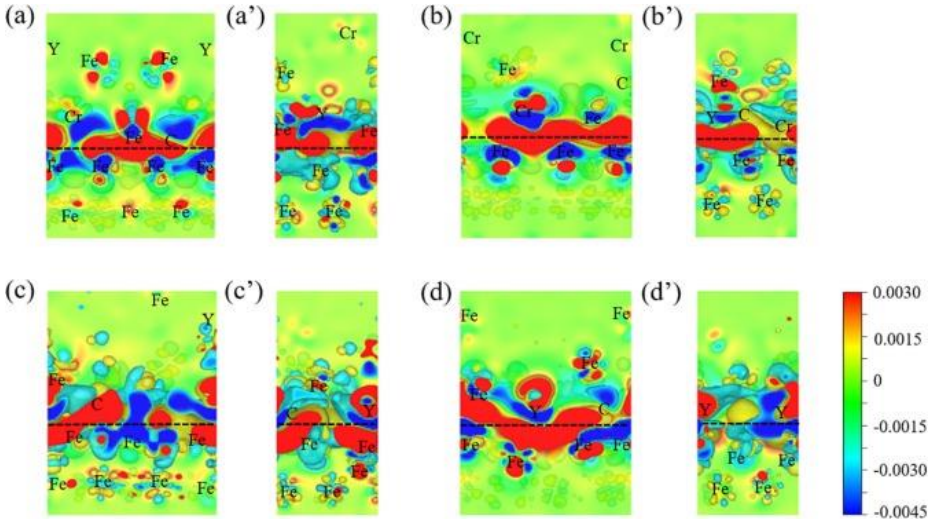

Fig. 4. Differential charge density of $Fe_3Cr_3YC_3(10\bar{1}0)//\gamma$-Fe(1 1 1) interface: (a) Fe-Fe; (b) Cr-Fe; (c) C-Fe; (d) Y-Fe.